

Wasserstein Regression with Empirical Measures and Density Estimation for Sparse Data

Yidong Zhou and Hans-Georg Müller

Department of Statistics, University of California, Davis
Davis, CA 95616, USA

July 27, 2023

Abstract

The problem of modeling the relationship between univariate distributions and one or more explanatory variables lately has found increasing interest. Traditional functional data methods cannot be applied directly to distributional data because of their inherent constraints. Modeling distributions as elements of the Wasserstein space, a geodesic metric space equipped with the Wasserstein metric that is related to optimal transport, is attractive for statistical applications. Existing approaches proceed by substituting proxy estimated distributions for the typically unknown response distributions. These estimates are obtained from available data but are problematic when for some of the distributions only few data are available. Such situations are common in practice and cannot be addressed with currently available approaches, especially when one aims at density estimates. We show how this and other problems associated with density estimation such as tuning parameter selection and bias issues can be side-stepped when covariates are available. We also introduce a novel version of distribution-response regression that is based on empirical measures. By avoiding the pre-processing step of recovering complete individual response distributions, the proposed approach is applicable when the sample size available for each distribution varies and especially when it is small for some of the distributions but large for others. In this case, one can still obtain consistent distribution estimates even for distributions with only few data by gaining strength across the entire sample of distributions, while traditional approaches where distributions or densities are estimated individually fail, since sparsely sampled densities cannot be consistently estimated. The proposed model is demonstrated to outperform existing approaches through simulations. Its efficacy is corroborated in two case studies on Environmental Influences on Child Health Outcomes (ECHO) data and eBay auction data.

KEY WORDS: distributional data analysis, Fréchet mean, multi-cohort study, optimal transport, sample of distributions, Wasserstein distance.

1 Introduction

Data consisting of samples of univariate probability distributions are increasingly prevalent across various research areas. Data that contain distributions as a basic unit of observation are encountered in the analysis of mortality (Chen et al. 2023; Ghodrati and Panaretos 2022), population pyramids (Hron et al. 2016; Bigot et al. 2017), brain connectivity (Petersen and Müller 2016), and financial returns (Zhang et al. 2022; Zhu and Müller 2023), among many other applications. This has led to the emerging field of distributional data analysis (Petersen et al. 2022). Distributions, represented as probability density functions, cumulative distribution functions or quantile functions, come with inherent constraints that are not present in traditional functional data. The space where distributions are situated is not a vector space, and linear methods developed for functional data cannot be directly applied. Various approaches have been proposed to address this challenge, including global transformations of univariate distributions to a Hilbert space (Hron et al. 2016; Petersen and Müller 2016), which however do not take the geometry of the space of distributions into account and are not isometric.

More recently, attention has focused on directly modeling distributions as elements of the Wasserstein space, a geodesic metric space related to optimal transport (Villani 2003; Panaretos and Zemel 2020). The pseudo-Riemannian structure of this space can be used to construct isometric exponential maps from the space to tangent bundles, where linear operations can be deployed (Bigot et al. 2017; Chen et al. 2023); however the inverse log map is not defined on the entire tangent space, which causes substantial difficulties and requires an ad-hoc constraint or projection step (Fletcher 2013; Pegoraro and Beraha 2022).

A commonly encountered problem is to model the relationship between distributions and one or more explanatory variables. Distribution-response regression problems arise in many modern data analysis settings. Examples include neuroimaging, where varying

patterns of brain connectivity distributions across age and other clinical covariates are of interest (Petersen and Müller 2016), metabolomics, where the aim is to model the dependence of a metabolite distribution on birth weight (Talská et al. 2018), and also mortality where one is interested in the dependence of age-at-death distributions on economic indicators (Petersen et al. 2022). Using the Wasserstein metric, distribution-response regression can be implemented as a special case of Fréchet regression (Petersen and Müller 2019), which models the relationship between random objects that lie in a generic metric space as responses and scalar or vector covariates as predictors.

In line with all local and global transformation methods, Fréchet regression requires that each distribution is observed as a distributional object. This is however usually unrealistic in practice as one rarely observes data samples where the atoms of the samples are entire distributions. Instead, one usually has samples of independent data $\{Y_{ij}\}_{j=1}^{N_i}$ that are generated by the distribution ν_i for each i ; see Figure 1 in Section 5.1 for a demonstration. To address this, current approaches for virtually all distributional data analysis methods include a prior distribution estimation step where one substitutes a smooth estimate for the unobservable distributional objects. Commonly this is done through a density estimate such as a kernel estimate or smoothed histogram that is obtained from data $\{Y_{ij}\}_{j=1}^{N_i}$ (Panaretos and Zemel 2016; Bigot et al. 2018; Petersen and Müller 2019) or a quantile function obtained by smoothing the empirical quantile function (Petersen et al. 2021; Gajardo and Müller 2021).

In the current literature, strong assumptions are used to ensure uniform convergence of density estimates, uniform across all random distributions (Panaretos and Zemel 2016; Petersen and Müller 2016; Petersen et al. 2021; Gajardo and Müller 2021). This preliminary smoothing step requires the minimum number of observations $m = m(n)$ that are generated by each random distribution, where n is the number of random distributions, to increase to infinity at a fast rate, typically faster than n . This entails convergence of the density estimation step at a rate that is faster than that of the

subsequent Fréchet regression or other operation so that the preliminary estimation step can be ignored in the overall asymptotic analysis. However, the assumption of a fast increase in the number of observations made for each of the distributions across the board is often unrealistic and the need to choose a tuning parameter for each distribution is another downside.

This state of affairs motivates the approach proposed in this paper, namely to use empirical measures $\hat{\nu}_i = (1/N_i) \sum_{j=1}^{N_i} \delta_{Y_{ij}}$, where $N_i \geq 1$ and $\delta_{Y_{ij}}$ denotes the Dirac measure at Y_{ij} , i.e., using the observations made for each random distribution directly, rather than first forming density estimates or other distributional estimates when conducting Fréchet regression. Besides avoiding the preliminary distribution estimation step with all its downsides, we will show that this has the further major benefit that it leads to a consistent density estimate for a distribution for which one has only very few observations, where the number of observations may not even increase with n and density estimation would normally be a hopeless enterprise. This becomes possible by harnessing the data across all distributions and exploiting the assumed smooth dependency of the response distributions on the predictors.

The proposed regression model, implemented through least common multiples and supported with asymptotic theory, avoids smoothing bias and tuning parameter choice in the pre-smoothing step and hence is more broadly applicable in practice, especially when the available sample size for each distribution greatly varies (Qiu et al. 2022). A typical example is provided by multi-cohort studies (O’Connor et al. 2022), where the availability and cost of observations highly varies across cohorts (Bonevski et al. 2014). We illustrate such a scenario with Environmental influences on Child Health Outcomes (ECHO) data (Knapp et al. 2023), where the dependence of body mass index distributions for children across cohorts on demographic covariates is of interest. A second example is provided by point processes, where distributions of event arrival times are inherently discretely observed with heterogeneous sample sizes. This scenario

is demonstrated with eBay auction data (Jank and Shmueli 2010), where we investigate the relationship between the bid time distribution and the opening bid.

The main innovations and strengths of the proposed approach are as follows. First, we illustrate that the universally employed pre-smoothing step is superfluous for distribution-response Fréchet regression; omitting this step avoids initial smoothing bias and tuning parameter selection and also avoids the requirement of a rapidly increasing number of observations per distribution. Second, we obtain consistent density estimates for densities with sparse number of observations by borrowing strength across the sample. Third, the proposed regression model is shown to outperform the existing smoothing approach in finite sample situations. Fourth, the proposed methods are supported by theory, including pointwise and uniform rates of convergence. Fifth, we demonstrate the utility and flexibility of the proposed distribution-response regression model.

The rest of the paper is organized as follows. In Section 2, we introduce some basic background and notations for the Wasserstein space of distributions. The proposed regression model for empirical measure responses and vector covariates is introduced in Section 3. Pointwise and uniform rates of convergence for the estimators are established in Section 4. Computational details and simulation results are presented in Section 5. The proposed framework is illustrated in Section 6 using the ECHO and eBay auction data. Detailed theoretical proofs are in the Appendix.

2 Preliminaries

For a closed interval Ω with Borel σ -algebra $\mathcal{B}(\Omega)$, we denote the set of probability measures, also referred to as measures or distributions, μ with domain Ω as $\mathcal{P}(\Omega)$ and define the space of measures with finite second moments as

$$\mathcal{W} := \left\{ \mu \in \mathcal{P}(\Omega); \int_{\Omega} x^2 \mu(dx) < \infty \right\}.$$

For any measure $\mu \in \mathcal{W}$ with cumulative distribution function F_μ , we consider the quantile function F_μ^{-1} to be the left continuous inverse of F_μ , i.e., $F_\mu^{-1}(\alpha) = \inf\{x \in \Omega : F_\mu(x) \geq \alpha\}$, for $\alpha \in (0, 1)$. The space \mathcal{W} is a metric space with the 2-Wasserstein, or simply Wasserstein distance between two measures $\mu_1, \mu_2 \in \mathcal{W}$ defined as

$$d_{\mathcal{W}}^2(\mu_1, \mu_2) := \inf_{\pi \in \Pi(\mu_1, \mu_2)} \int_{\Omega \times \Omega} |x - y|^2 d\pi(x, y),$$

where $\Pi(\mu_1, \mu_2)$ is the set of joint measures on $\Omega \times \Omega$ with marginals μ_1 and μ_2 (Kantorovich 1942). It is well known (Villani 2003) that the Wasserstein distance can be expressed as the L^2 distance between the corresponding quantile functions,

$$d_{\mathcal{W}}^2(\mu_1, \mu_2) = \int_0^1 \{F_{\mu_1}^{-1}(\alpha) - F_{\mu_2}^{-1}(\alpha)\}^2 d\alpha. \quad (1)$$

It can be shown that \mathcal{W} endowed with $d_{\mathcal{W}}$ is a complete and separable metric space, the Wasserstein space (Panaretos and Zemel 2020; Villani 2003).

Consider a random element ν taking values in the Wasserstein space \mathcal{W} , assumed to be square integrable in the sense that $E\{d_{\mathcal{W}}^2(\nu, \mu)\} < \infty$ for all $\mu \in \mathcal{W}$. The Fréchet mean of ν (Fréchet 1948), extending the usual notion of mean, is

$$\nu_{\oplus} = \arg \min_{\mu \in \mathcal{W}} E\{d_{\mathcal{W}}^2(\nu, \mu)\},$$

which is well-defined and unique as the Wasserstein space \mathcal{W} is a Hadamard space (Kloeckner 2010). It follows from (1) that the quantile function of the Fréchet mean ν_{\oplus} is $F_{\nu_{\oplus}}^{-1}(\cdot) = E\{F_{\nu}^{-1}(\cdot)\}$. In the following, the notation μ refers to fixed measures in \mathcal{W} , ν to random measures, $a \lesssim b$ means that there exists a positive constant C such that $a \leq Cb$ and $a \asymp b$ that $a \lesssim b$ and $b \lesssim a$. The Euclidean norm in \mathbb{R}^p is denoted by $\|\cdot\|_E$.

3 Wasserstein Regression with Empirical Measures

Let (Z, ν) be a random pair with joint distribution \mathcal{F} on the product space $\mathbb{R}^p \times \mathcal{W}$. Denote the mean and variance of Z by $\theta = E(Z)$ and $\Sigma = \text{Var}(Z)$, with Σ strictly positive definite. To model the regression relation between random measures ν and vector covariates Z , we adopt the framework of Fréchet regression, a version of conditional Fréchet means designed for the regression of metric space-valued responses on Euclidean predictors (Petersen and Müller 2019; Chen and Müller 2022). Fréchet regression targets the conditional Fréchet mean of ν given $Z = z$,

$$m(z) = \arg \min_{\mu \in \mathcal{W}} E\{d_{\mathcal{W}}^2(\nu, \mu) | Z = z\}.$$

A brief description of Fréchet regression is as follows; for more details see Petersen and Müller (2019). Suppose that $\{(Z_i, \nu_i)\}_{i=1}^n$ are n independent realizations of (Z, ν) with

$$\bar{Z} = \frac{1}{n} \sum_{i=1}^n Z_i, \quad \hat{\Sigma} = \frac{1}{n} \sum_{i=1}^n (Z_i - \bar{Z})(Z_i - \bar{Z})^T.$$

Global Fréchet regression can be considered as a generalization of classical multiple linear regression for real-valued responses and targets

$$m_G(z) = \arg \min_{\mu \in \mathcal{W}} E\{s_G(z) d_{\mathcal{W}}^2(\nu, \mu)\}, \quad (2)$$

with weight function $s_G(z) = 1 + (Z - \theta)^T \Sigma^{-1} (z - \theta)$ and empirical version

$$\tilde{m}_G(z) = \arg \min_{\mu \in \mathcal{W}} \frac{1}{n} \sum_{i=1}^n s_{iG}(z) d_{\mathcal{W}}^2(\nu_i, \mu), \quad (3)$$

for a sample $\{(Z_i, \nu_i)\}_{i=1}^n$, where $s_{iG}(z) = 1 + (Z_i - \bar{Z})^T \hat{\Sigma}^{-1} (z - \bar{Z})$.

Analogously, local Fréchet regression extends local linear regression to metric space-

valued responses. For the special case of a scalar predictor $Z \in \mathbb{R}$ it targets

$$m_{L,h}(z) = \arg \min_{\mu \in \mathcal{W}} E\{s_L(z, h)d_{\mathcal{W}}^2(\nu, \mu)\}, \quad (4)$$

where $s_L(z, h) = K_h(Z-z)[u_2 - u_1(Z-z)]/\sigma_0^2$, $u_j = E[K_h(Z-z)(Z-z)^j]$ for $j = 0, 1, 2$, $\sigma_0^2 = u_0u_2 - u_1^2$, and $K_h(\cdot) = h^{-1}K(\cdot/h)$ with $K(\cdot)$ a continuous symmetric probability density function on $[-1, 1]$ and h a bandwidth and with empirical version

$$\tilde{m}_{L,h}(z) = \arg \min_{\mu \in \mathcal{W}} \frac{1}{n} \sum_{i=1}^n s_{iL}(z, h)d_{\mathcal{W}}^2(\nu_i, \mu). \quad (5)$$

Here $s_{iL}(z, h) = K_h(Z_i-z)[\hat{u}_2 - \hat{u}_1(Z_i-z)]/\hat{\sigma}_0^2$, where $\hat{u}_j = n^{-1} \sum_{i=1}^n K_h(Z_i-z)(Z_i-z)^j$ for $j = 0, 1, 2$ and $\hat{\sigma}_0^2 = \hat{u}_0\hat{u}_2 - \hat{u}_1^2$.

In previous work on Fréchet regression (Petersen and Müller 2019), response distributions in the Wasserstein space \mathcal{W} served as one of the key examples but it has been typically assumed that the measures are fully observed while at the same time they may be randomly perturbed in analogy to usual additive noise models (Chen and Müller 2022). However none of this applies in the more realistic situation where one has data $\{Y_{ij}\}_{j=1}^{N_i}$ that are generated from each distribution ν_i . The stopgap solution applied previously is a preprocessing density estimation step (Panaretos and Zemel 2016; Petersen and Müller 2016), where it is assumed that the number of data available for all measures increases at a faster rate than the available number of observation points (Z_i, ν_i) in order to preserve asymptotic convergence rates.

However the intermediate kernel density estimates will be biased and inconsistent if some of the measures generate only very few observations, which then renders this approach infeasible. This provides the motivation to replace the unobservable measures ν_i with the empirical measure $\hat{\nu}_i = (1/N_i) \sum_{j=1}^{N_i} \delta_{Y_{ij}}$. This circumvents the pre-smoothing step and hence eliminates the corresponding tuning parameter selection and smoothing bias. Using empirical measures $\hat{\nu}_i$ in lieu of the unobservable measures ν_i as responses,

the approaches proposed here are the global and local Regression with Empirical Measures (REM), replacing (3) and (5) by

$$\hat{m}_G(z) = \arg \min_{\mu \in \mathcal{W}} \frac{1}{n} \sum_{i=1}^n s_{iG}(z) d_{\mathcal{W}}^2(\hat{\nu}_i, \mu), \quad (6)$$

$$\hat{m}_{L,h}(z) = \arg \min_{\mu \in \mathcal{W}} \frac{1}{n} \sum_{i=1}^n s_{iL}(z, h) d_{\mathcal{W}}^2(\hat{\nu}_i, \mu). \quad (7)$$

The computation of the minimizers in (6) and (7) is not straightforward, as some of the weights in these minimization problems are inherently negative. We show in Section 5.1 that adopting least common multiples leads to a simple and efficient algorithm.

4 Asymptotic Properties

We establish pointwise and uniform rates of convergence under the framework of M-estimation. Denote by \mathcal{W}^{ac} the set of measures $\mu \in \mathcal{W}$ that are absolutely continuous with respect to the Lebesgue measure dx on \mathbb{R} . To establish rates of convergence for estimates (6) and (7), we require the following conditions.

- (C1) The random measure ν satisfies $\nu \in \mathcal{W}^{\text{ac}}$ and its probability density function f_ν is bounded below by a positive constant.
- (C2) The sample size N_i is independently Poisson distributed with parameter $c_i \lambda_n$ where $c_i \geq c > 0$ are constants and $0 < \lambda_n / \log n \rightarrow \infty$ as $n \rightarrow \infty$.

Condition (C1) ensures the random measure ν is well-behaved. Since measures ν_i are discretely observed, rates of convergence will be affected by the rate at which the sample size N_i increases to infinity. Instead of directly requiring the sample size N_i to diverge to infinity, Condition (C2) imposes a distributional condition on N_i . This set-up reflects the case of heterogeneous sample sizes, as it allows some sample sizes N_i to be very small and even 0 for some of the observed distributions, but also ensures that

the N_i are positive almost surely for large enough n ; compare Lemma 3 in Panaretos and Zemel (2016). The following result formalizes the consistency of the proposed global REM estimates and provides rates of convergence.

Theorem 1. *Under Conditions (C1) and (C2), the global REM estimate defined in (6) satisfies*

$$d_{\mathcal{W}}\{\hat{m}_G(z), m_G(z)\} = O_p(n^{-1/2} + \lambda_n^{-1/2}).$$

Furthermore, for any constant B it holds that for any $\varepsilon > 0$,

$$\sup_{\|z\|_E \leq B} d_{\mathcal{W}}\{\hat{m}_G(z), m_G(z)\} = O_p(n^{-1/\{2(1+\varepsilon)\}} + \lambda_n^{-1/2}).$$

All proofs are in the Appendix. The pointwise rate of convergence is $O_p(n^{-1/2})$ as long as the sample size N_i , on average, grows at the same rate as n , i.e., $\lambda_n \asymp n$, which is the same as the well-known optimal rate for multiple linear regression. Similarly we obtain the following result for local REM, where the kernel and distributional assumptions (A1)–(A4) listed in the Appendix A are standard for local regression.

Theorem 2. *Under Conditions (C1) and (C2), the local REM estimate defined in (7) satisfies*

$$d_{\mathcal{W}}\{\hat{m}_{L,h}(z), m(z)\} = O_p(n^{-2/5} + \lambda_n^{-1/2})$$

for $h \sim n^{-1/5}$ if Assumptions (A1) and (A2) hold. Furthermore, for a closed interval $\mathcal{T} \subset \mathbb{R}$,

$$\sup_{z \in \mathcal{T}} d_{\mathcal{W}}\{\hat{m}_{L,h}(z), m(z)\} = O_p(n^{-1/(3+\varepsilon)} + \lambda_n^{-1/2})$$

for $h \sim n^{-1/(6+2\varepsilon)}$ and any $\varepsilon > 0$ if Assumptions (A3) and (A4) hold.

As long as $\lambda_n \asymp n^{4/5}$, the local REM estimate achieves the pointwise rate $O_p(n^{-2/5})$, corresponding to the well-known optimal rate for standard local linear regression.

5 Implementation and Simulations

5.1 Implementation details

To implement the proposed methods, one needs to solve minimization problems (6) and (7). By standard properties of the $L^2(0, 1)$ inner product, (6) and (7) can be simplified to

$$\begin{aligned}\hat{m}_G(z) &= \arg \min_{\mu \in \mathcal{W}} d_{L^2}^2\{\hat{B}_G(z), F_\mu^{-1}\}, \\ \hat{m}_{L,h}(z) &= \arg \min_{\mu \in \mathcal{W}} d_{L^2}^2\{\hat{B}_{L,h}(z), F_\mu^{-1}\},\end{aligned}\tag{8}$$

where $\hat{B}_G(z) = n^{-1} \sum_{i=1}^n s_{iG}(z) F_{\hat{\nu}_i}^{-1}$, $\hat{B}_{L,h}(z) = n^{-1} \sum_{i=1}^n s_{iL}(z, h) F_{\hat{\nu}_i}^{-1}$ and $d_{L^2}(\cdot, \cdot)$ denotes the L^2 distance; see the proof of Theorem 1 for details. The minimizers $\hat{m}_G(z)$ and $\hat{m}_{L,h}(z)$, viewed as projections onto \mathcal{W} , exist and are unique for any z by convexity and closedness of \mathcal{W} . To tackle the challenge of substantial variation in the number of jumps for empirical quantile functions $F_{\hat{\nu}_i}^{-1}$ due to varying sample sizes N_i , we propose an algorithm based on the least common multiple, which allows us to compute $\hat{B}_G(z)$ and $\hat{B}_{L,h}(z)$ as straightforward weighted averages. The algorithm for global REM is outlined in Algorithm 1. The only difference for local REM is the substitution of the weight function $s_{iL}(z, h)$ for $s_{iG}(z)$.

In the first step of Algorithm 1, one needs to calculate $M = \text{lcm}(\{N_i\}_{i=1}^n)$, the least common multiple of the ensemble $\{N_i\}_{i=1}^n$. To control the size of $\text{lcm}(\{N_i\}_{i=1}^n)$ especially when n is large and N_i greatly varies, we incorporate a threshold $M = \min\{\text{lcm}(\{N_i\}_{i=1}^n), M_0\}$, where M_0 is a pre-specified constant, say 5,000. The fifth step of Algorithm 1 involves a minimization problem to obtain the projection onto \mathcal{W} . For this step, we use a Riemann sum approximation of the L^2 distance. This leads to

Algorithm 1: Global REM

Input: data $\{(Z_i, \{Y_{ij}\}_{j=1}^{N_i})\}_{i=1}^n$, and a new predictor level z .

Output: prediction $\hat{m}_G(z)$.

- 1 $M \leftarrow$ the least common multiple of $\{N_i\}_{i=1}^n$;
 - 2 $\{\mathbb{V}_i\}_{i=1}^n \leftarrow$ for each $i = 1, \dots, n$, stretch $(Y_{i1}, \dots, Y_{iN_i})^\top$ to a vector of length M , $\mathbb{V}_i = (V_{i1}, \dots, V_{iM})^\top$, by repeating each element $\frac{M}{N_i}$ times and then arranging in ascending order;
 - 3 $s_{iG}(z) \leftarrow 1 + (Z_i - \bar{Z})^\top \hat{\Sigma}^{-1}(z - \bar{Z})$ where $\bar{Z} = \frac{1}{n} \sum_{i=1}^n Z_i$ and $\hat{\Sigma} = \frac{1}{n} \sum_{i=1}^n (Z_i - \bar{Z})(Z_i - \bar{Z})^\top$ are the sample mean and variance of $\{Z_i\}_{i=1}^n$, respectively;
 - 4 $\bar{\mathbb{V}} = (\bar{V}_1, \dots, \bar{V}_M)^\top \leftarrow \frac{1}{n} \sum_{i=1}^n s_{iG}(z) \mathbb{V}_i$, the element-wise weighted average of $\{\mathbb{V}_i\}_{i=1}^n$;
 - 5 $\hat{m}_G(z) \leftarrow \arg \min_{\mu \in \mathcal{W}} d_{L^2}^2(\hat{B}_G(z), F_\mu^{-1})$, where $\hat{B}_G(z) = \sum_{m=1}^M \bar{V}_m \mathbf{1}_{q \in (\frac{m-1}{M}, \frac{m}{M}]}$ is a step function defined on $q \in [0, 1]$.
-

the following convex quadratic optimization problem,

$$\begin{aligned}
 & \text{minimize} && \sum_{m=1}^M (q_m - \bar{V}_m)^2 \\
 & \text{subject to} && q_1 \leq q_2 \leq \dots \leq q_{M-1} \leq q_M, \\
 & && q_j \in \Omega, \quad j = 1, \dots, M.
 \end{aligned} \tag{9}$$

The solution q^* represents a discretized version of the predicted quantile function. We use the `osqp` package (Stellato et al. 2020) in R to solve the optimization problem presented in (9).

An illustrative example is in Figure 1 to demonstrate the proposed approach and algorithm for the case of global REM. In the top left panel of Figure 1, we depict large variation in sample sizes N_i of the observations available for distributions ν_i , where the smallest N_i is $N_i = 1$. A simple calculation shows that the global weight function is $s_{iG}(z) = 1 + (2i - 5)(z - 5)/5$ for $i = 1, 2, 3, 4$. The predicted distribution at predictor level z is obtained by calculating $\hat{B}_G(z)$ in (8), a weighted average of empirical quantile functions $F_{\nu_i}^{-1}$, see the top right panel of Figure 1, utilizing weights $s_{iG}(z)$, followed by

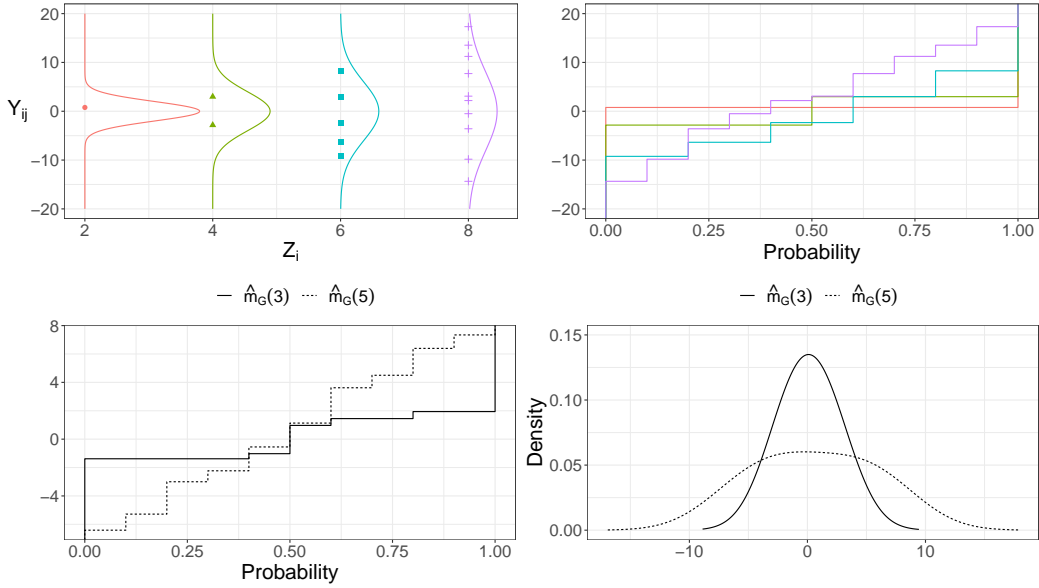


Figure 1: Illustrating global REM, where N_i observations $\{Y_{ij}\}_{j=1}^{N_i}$ are sampled from distributions $\nu_i = N(0, Z_i^2)$ for $i = 1, 2, 3, 4$, with sample sizes $N_1 = 1, N_2 = 2, N_3 = 5, N_4 = 10$ and scalar covariates $Z_1 = 2, Z_2 = 4, Z_3 = 6, Z_4 = 8$. Top left: Visualization of Y_{ij} versus covariate levels Z_i , along with the underlying true densities. Top right: Empirical quantile functions corresponding to the empirical measures $\hat{\nu}_i = (1/N_i) \sum_{j=1}^{N_i} \delta_{Y_{ij}}$. Bottom: Predicted quantile functions (left) and corresponding densities (right), obtained with global REM for predictor levels $z = 3$ and $z = 5$.

a projection onto \mathcal{W} . The weighted average is implemented with Algorithm 1. The predicted distribution $\hat{m}_G(z)$ obtained in Algorithm 1 is represented as an empirical quantile function, which can subsequently be converted into a density function for improved visualization. We adopted the `qf2pdf` function in the `frechet` package (Chen et al. 2020) to construct densities from quantile functions in this example and for our data applications; there are also alternative options (Niles-Weed and Berthet 2022).

The bottom two panels of Figure 1 illustrate the predicted distributions using global REM for predictor levels $z = 3$ and $z = 5$. For $z = \bar{Z} = 5$, one obtains the Wasserstein barycenter of the four empirical measures as for this case the global weight function is constant, i.e., $s_{iG}(5) = 1$ for all i . Since $z = 3$ is close to the left endpoint, the estimation requires negative weights where $s_{4G}(3) = -1/5$. In the presence of negative weights, $\hat{B}_G(3)$ no longer resides in \mathcal{W} , necessitating the additional projection step as

per (8).

5.2 Simulations

To assess the finite sample performance of the proposed methods, we construct a generative model that produces random responses ν along with an Euclidean predictor $Z \in \mathbb{R}$. Consider the true regression function $m(Z)$, represented as quantile function,

$$m(Z) = E(\eta|Z) + E(\sigma|Z)\Phi^{-1}(\cdot),$$

which corresponds to a Gaussian distribution with mean and standard deviation depending on Z . The distribution parameters of the true regression function $m(Z)$ are generated conditionally on Z , where the mean and the standard deviation are assumed to follow a normal distribution and a Gamma distribution, respectively. Four different simulation settings are examined as summarized in Table 1. In Settings I and II, the response is generated, on average, as a Gaussian distribution with parameters depending on Z . Setting I corresponds to a global scenario where the response ν depends linearly on the predictor Z as $E(\eta|Z) = \eta_0 + \alpha Z$ and $E(\sigma|Z) = \sigma_0 + \beta Z$. In Setting II, the nonlinear relationships $E(\eta|Z) = \eta_0 + \alpha \sin(\pi Z)$ and $E(\sigma|Z) = \sigma_0 + \beta \sin(\pi Z)$ is considered for the true underlying regression model.

To take non-Gaussian distributions into consideration, we apply an additional transportation to the random response in Settings III and IV. Specifically, after sampling the distribution parameters as in the previous settings, the resulting distribution is transported in Wasserstein space via a random transport map T , uniformly sampled from the collection of maps $T_k(\alpha) = \alpha - \sin(k\alpha)/|k|$ for $k \in \{-2, -1, 1, 2\}$ (Panaretos and Zemel 2016). Such a transportation significantly complicates Settings III and IV and makes the response distribution non-Gaussian. One can show that the true regression function remains the same after this random transportation.

Table 1: Four simulation settings, where F_ν^{-1} represents the quantile function of the generated random response. The distribution parameters of the random response depend on the predictor Z as indicated for Settings I–IV. An additional transport map T , uniformly sampled from the collection of maps $T_k(\alpha) = \alpha - \sin(k\alpha)/|k|$ for $k \in \{-2, -1, 1, 2\}$, is applied to the resulting random responses in Settings III and IV.

	Type	Setting
I	global model	$F_\nu^{-1}(\cdot) = \eta + \sigma\Phi^{-1}(\cdot)$, where $\eta Z \sim N(\eta_0 + \alpha Z, \tau^2)$ and $\sigma Z \sim \text{Gamma}[\{\sigma_0 + \beta Z\}^2/\kappa, \kappa/\{\sigma_0 + \beta Z\}]$
II	local model	$F_\nu^{-1}(\cdot) = \eta + \sigma\Phi^{-1}(\cdot)$, where $\eta Z \sim N(\eta_0 + \alpha \sin(\pi Z), \tau^2)$ and $\sigma Z \sim \text{Gamma}[\{\sigma_0 + \beta \sin(\pi Z)\}^2/\kappa, \kappa/\{\sigma_0 + \beta \sin(\pi Z)\}]$
III	global model with random transport	$F_\nu^{-1}(\cdot) = T \circ \{\eta + \sigma\Phi^{-1}(\cdot)\}$, where $\eta Z \sim N(\eta_0 + \alpha Z, \tau^2)$ and $\sigma Z \sim \text{Gamma}[\{\sigma_0 + \beta Z\}^2/\kappa, \kappa/\{\sigma_0 + \beta Z\}]$
IV	local model with random transport	$F_\nu^{-1}(\cdot) = T \circ \{\eta + \sigma\Phi^{-1}(\cdot)\}$, where $\eta Z \sim N(\eta_0 + \alpha \sin(\pi Z), \tau^2)$ and $\sigma Z \sim \text{Gamma}[\{\sigma_0 + \beta \sin(\pi Z)\}^2/\kappa, \kappa/\{\sigma_0 + \beta \sin(\pi Z)\}]$

We consider $n = 50, 100, 200, 500, 1000$, with $Q = 1000$ Monte Carlo runs for each of the four simulation settings. For each n , the sample size N_i is independently sampled from the Poisson distribution with parameter $0.25n$. In each Monte Carlo run, predictors $\{Z_i\}_{i=1}^n$ are independently sampled from $U(-1, 1)$. For each i , mean and standard deviation of ν_i are generated conditionally on Z_i as described in Table 1, with $\eta_0 = 0, \sigma_0 = 3, \alpha = 3, \beta = 0.5, \tau = 0.5$, and $\kappa = 1$. N_i random observations $\{Y_{ij}\}_{j=1}^{N_i}$ are then independently sampled from ν_i . For the q th Monte Carlo run for a given setting, the quality of the estimation is quantified by the integrated squared error (ISE)

$$\text{ISE}_q = \int_{-1}^1 d_{\mathcal{W}}^2\{\hat{m}_q(z), m(z)\} dz,$$

where $m(\cdot)$ is the true regression function and $\hat{m}_q(z)$ is the fitted regression function. The bandwidths for the local REM in the second simulation setting are chosen as $n^{-1/5}$.

We also include comparisons with the previous two-step procedures that included a

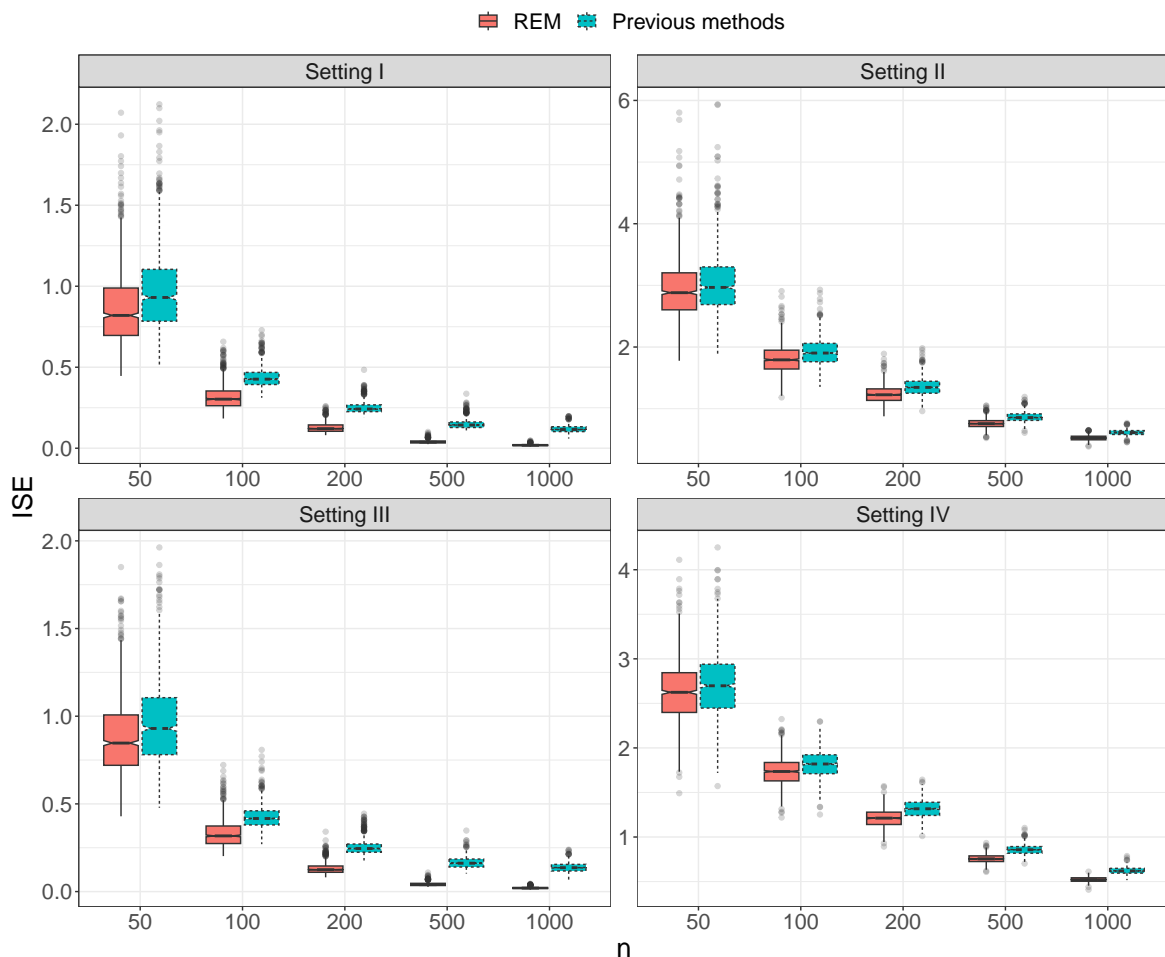


Figure 2: Boxplots of integrated square errors (ISE) for $Q = 1000$ Monte Carlo runs and different simulation settings using the proposed REM (red) and the two-step approaches that were adopted previously (blue).

prior kernel smoothing step (Panaretos and Zemel 2016; Petersen and Müller 2019) to estimate the densities of the ν_i from the available discrete observations. The integrated squared errors (ISE) for all Monte Carlo runs and different n under the four simulation settings using the proposed methods and the comparison methods are summarized in the boxplots in Figure 2. With increasing sample size, ISE is seen to decrease for all simulation settings, demonstrating the convergence of the proposed methods to the target. Importantly, the proposed REM outperforms the comparison methods under all simulation settings. Indeed, the preliminary smoothing step required in the previous

literature involved a unnecessary tuning parameter selection and fails when the data for some measures are very sparse.

6 Data Applications

6.1 Cohort-specific BMI distribution for US preschool children

The Environmental influences on Child Health Outcomes (ECHO) program is an NIH-funded nationwide consortium of multiple cohort studies across the United States designed to investigate the effects of early life exposures on child health and development (Gillman and Blaisdell 2018). The ECHO program combines existing prenatal and pediatric data collected via cohort-specific protocols with a standardized ECHO-wide protocol that was established in 2019 (Knapp et al. 2023). The de-identified data on participants contributing extant and new data can be accessed through the National Institute of Child Health and Human Development (NICHD) Data and Specimen Hub (DASH); the version we use here has been made available on August 31, 2021 (Gillman 2022). As a multi-cohort study, ECHO brings separate cohorts together so that researchers can access information from a large and diverse population of children followed from the prenatal period through adolescence.

It is of interest to study the role of demographic factors in child development, measured in terms of body mass index (BMI), calculated as weight in kilograms divided by height in meters squared. We extracted weight and height measurements of preschool children aged approximately 4 years for 17 cohorts from ECHO, along with demographic information for each cohort, aiming to shed light on how the distribution of BMI of preschool children varies across different cohorts in relation to cohort-specific demographic characteristics. The responses specifically are the cohort-specific distributions of BMI for 4-year-old children in the respective cohort. Cohort-specific covariates that reflect important demographic characteristics of each cohort include average BMI

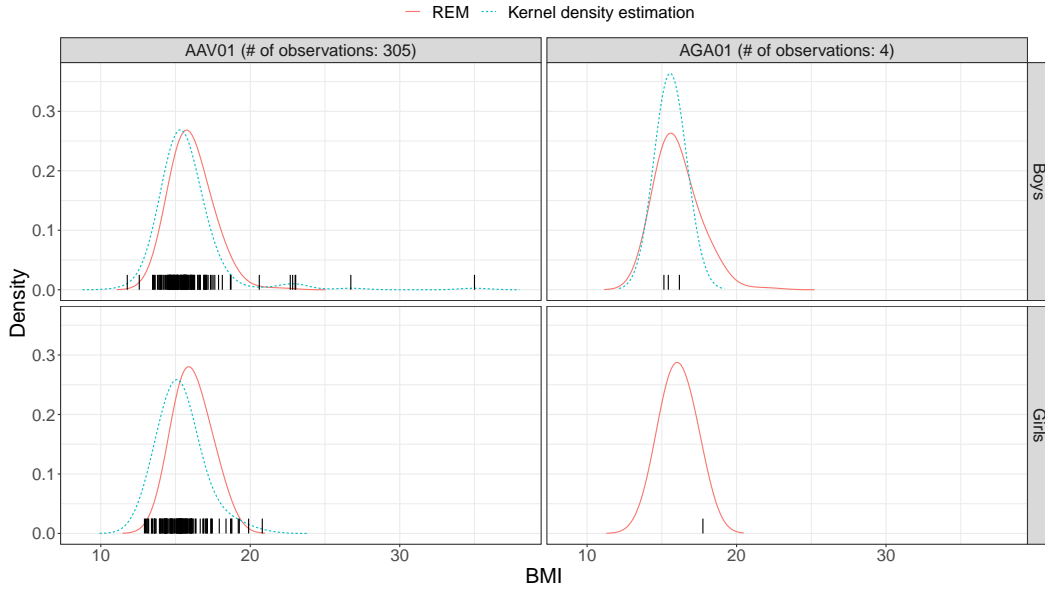
Table 2: Number of weight and height measurements for each cohort.

Cohort	AAA01	AAD01	AAE01	AAF01	AAJ01	AAU01	AAV01	AAW02
Boys	139	70	77	35	9	10	160	12
Girls	101	70	81	15	7	8	145	8
Total	240	140	158	50	16	18	305	20
AAX04	AAX06	ADA01	AGA01	AJA02	AJA03	AKA01	AKA02	ALA01
83	124	8	3	44	6	7	76	134
67	110	7	1	38	14	3	71	128
150	234	15	4	82	20	10	147	262

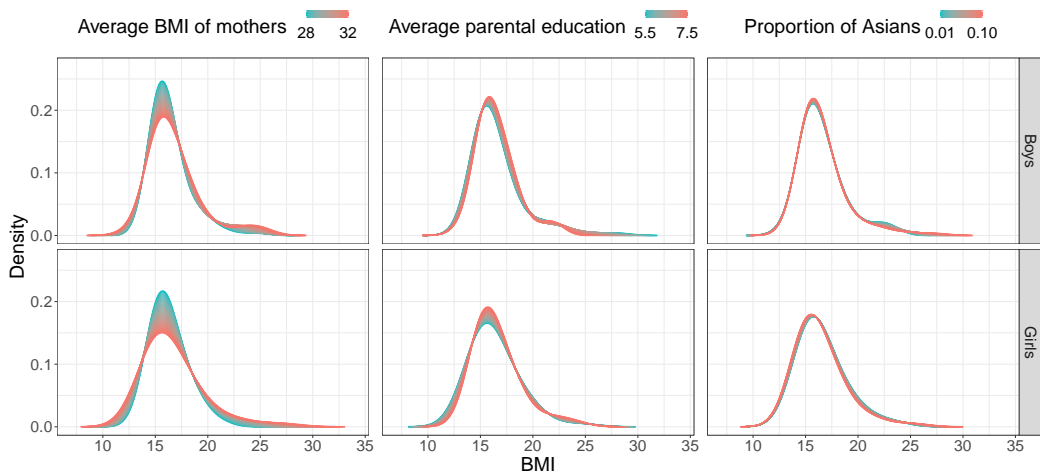
of mothers, average parental education and proportion of Asians.

Due to differences in the cost and accessibility of visits for different cohorts, there is a significant variation in sample size for each cohort. The amount of accessible weight and height measurements for each cohort varies substantially as a result; see Table 2 for further information. Specifically, there is only one weight and height measurement for girls in AGA01 cohort, while 160 measurements are available for boys in AAV01 cohort. We applied global REM to boys and girls separately. The fitted BMI densities for two cohorts with the most and least weight and height measurements (AAV01, AGA01) are demonstrated in Figure 3(a), along with the corresponding BMI measurements shown as ticks. Although only one measurement is available for girls in the AGA01 cohort, the proposed regression model is able to borrow information from cohorts with more measurements to construct a reasonable density estimate. We also include kernel density estimates in Figure 3(a) for comparison, where the covariate information is not taken into account. Note that kernel density estimation is infeasible for girls in the AGA01 cohort since only one observation is available.

To further investigate the effects of different demographic factors, predicted BMI densities at different predictor levels are shown in Figure 3(b). Separately for each predictor, the predictor level was varied from the first to the third quantile of the sample, while the other two predictors were held fixed at their median level. We observe that the average BMI of mothers is the most influential predictor, where with increasing



(a)



(b)

Figure 3: (a) Fitted densities of BMI distributions (solid) of US preschool boys and girls for AAV01 and AGA01 cohorts, along with direct kernel density estimates (dashed). The corresponding BMI measurements are shown as ticks. (b) Predicted BMI densities of US preschool boys and girls at different predictor levels.

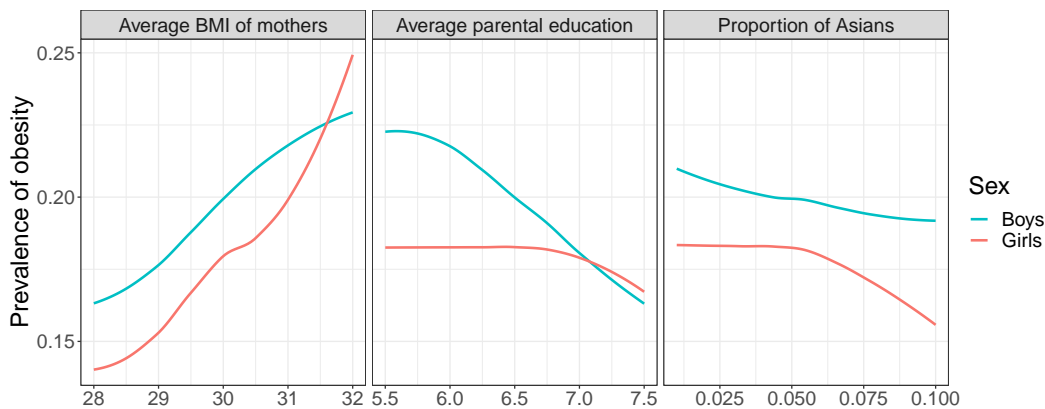


Figure 4: Prevalence of obesity for US preschool boys and girls at different predictor levels.

average BMI of mothers, the BMI distribution for both 4-year-old boys and girls flattens out and becomes less concentrated. For the predictor average parental education, higher values are associated with heavier tails of the BMI distribution for both 4-year-old boys and girls. For higher average parental education, the BMI distribution of boys also shifts a little to the right. The proportion of Asians in the population seems to have little effect on the BMI distribution of preschool children.

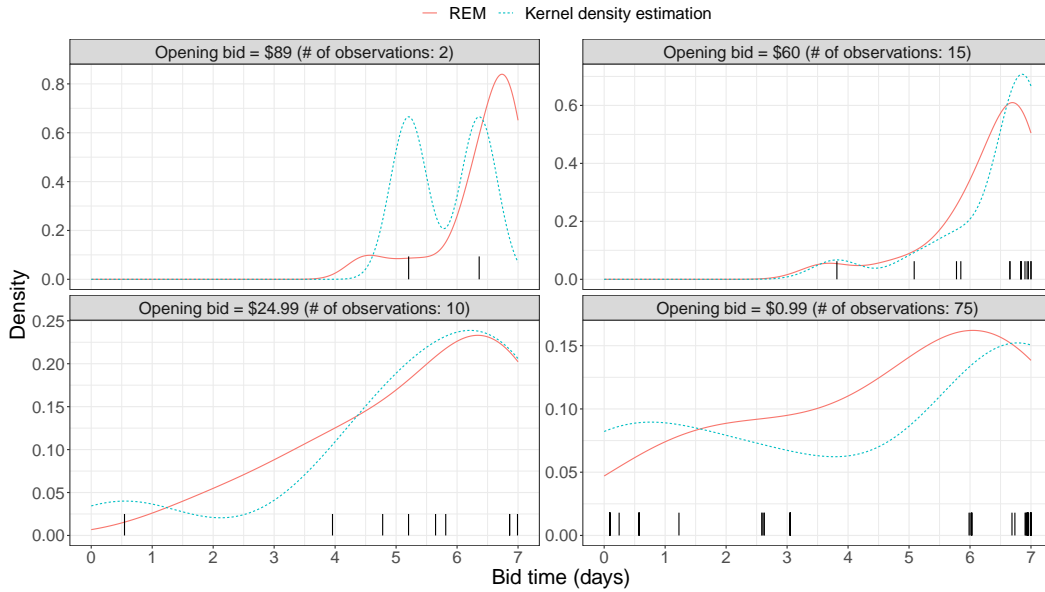
Childhood obesity is continuing to rise in the US, and currently about 13.7 million children are considered to be overweight/obese. For the ECHO data, we can compute the probability of obesity from the BMI distribution to investigate demographic disparities in early childhood obesity. Obesity is defined as a BMI at or above the 95th percentile for children of the same age and sex. According to the sex-specific BMI-for-age 2000 CDC Growth Charts, the BMI threshold for a 4-year-old boy to be obese is 17.8, while for girl the value is 18. Based on the predicted BMI distributions (see Figure 3), we calculated the corresponding probabilities of obesity at different predictor levels, with results illustrated in Figure 4. The average BMI of mothers is found to be positively correlated with the prevalence of obesity among four-year-old children, while average parental education and proportion of Asians are negatively associated

with obesity. None of these associations establishes a causal effect, but these findings are in agreement with the current literature on obesity, where parental overweight and low socioeconomic status were found to be strong risk factors of obesity in children (Danielzik et al. 2004; Vazquez and Cubbin 2020), while obesity is less common in Asian children (Anderson and Whitaker 2009).

6.2 Bid time distribution for eBay auction data

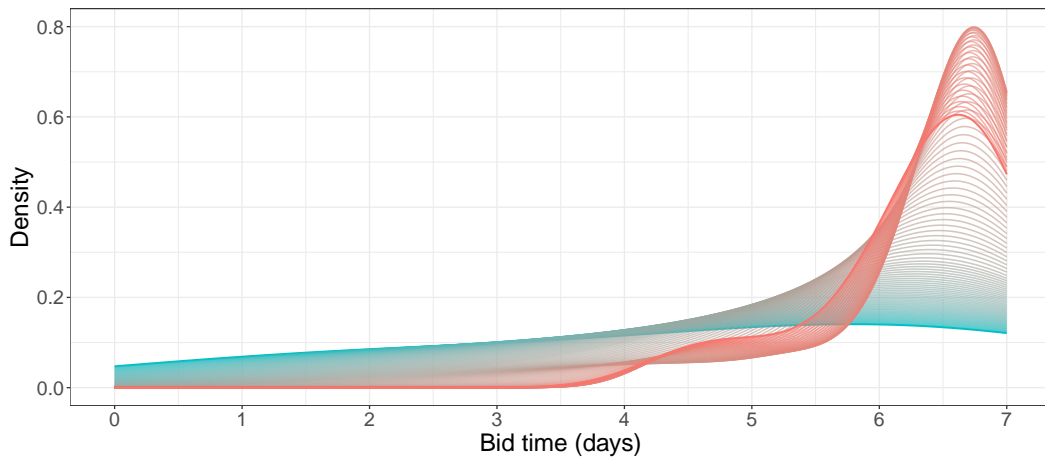
Electronic commerce and in particular eBay, with the prevalence of online auction, is a rich data source for the study of bidding behavior and strategies (Wang et al. 2008; Liu and Müller 2009; Liu et al. 2019). Here we implemented the proposed regression model to analyze eBay auction data consisting of 93 7-day auctions for an Xbox game console. The data are publicly available at <https://www.modelingonlineauctions.com/datasets> (Jank and Shmueli 2010). For each auction, the opening bid set by the seller serves as predictor and the time stamps where bids were placed as responses. We aim to investigate the dependence of bid time distribution on the opening bid. The number of bids for each auction varies from 2 to 75, necessitating the application of the proposed regression model, for which we used local REM.

The fitted bid time densities for four auctions including the two with the most and least bids are illustrated in Figure 5(a). The corresponding bid times are shown as ticks for comparison. We find that the proposed regression model is robust to the strong heterogeneity inherent in the auction data, where for example the bid time density for an auction with only two bids (top left panel in Figure 5(a)) is reasonably well recovered. In contrast, standard kernel density estimation implemented separately for each auction lacks the ability to borrow strength across the entire sample of distributions and, as expected, fails to reconstruct the underlying bid time density for the auction with only two bids. To further investigate the effect of the opening bid amount on the bid time distribution, we show in Figure 5(b) the predicted bid time densities for



(a)

Opening bid █ █
1 100



(b)

Figure 5: (a) Fitted bid time densities (solid) for four different auctions of an Xbox game console with the proposed method, along with auction-specific kernel density estimates (dashed). The corresponding bid times are shown as ticks. (b) Predicted bid time densities for different opening bids.

opening bids varying from 1 to 100 dollars. Bidders tend to bid late in the auction if the opening bid set by the seller is high. In contrast, if the opening bid is low, bid time is more evenly distributed over the 7-day period. Regardless of the opening bid, bid sniping is prevalent, where the bidding becomes frenzied near the end of an auction. A lower opening bid is associated with less bid sniping in the sense that bidding is more spread out over the entire time range of the auction.

Acknowledgements

We acknowledge support from NSF grants DMS-20146260, DMS-2310450 and IOS-2102953.

Appendix A. Assumptions for Theorem 1 and Theorem 2

In the following, $f_Z(\cdot)$ and $f_{Z|\nu}(\cdot, \mu)$ stand for the marginal density of Z and the conditional density of Z given $\nu = \mu$, respectively, and \mathcal{T} is a closed interval in \mathbb{R} with interior \mathcal{T}° .

(A1) The kernel $K(\cdot)$ is a probability density function, symmetric around zero. Furthermore, defining $K_{kj} = \int_{\mathbb{R}} K^k(u)u^j du$, $|K_{14}|$ and $|K_{26}|$ are both finite.

(A2) $f_Z(\cdot)$ and $f_{Z|\nu}(\cdot, \mu)$ both exist and are twice continuously differentiable, the latter for all $\mu \in \mathcal{W}$, and $\sup_{z, \mu} |(\partial^2 f_{Z|\nu} / \partial z^2)(z, \mu)| < \infty$. Additionally, for any open set $U \subset \mathcal{W}$, $\int_U dF_{\nu|Z}(z, \mu)$ is continuous as a function of z .

(A3) The kernel $K(\cdot)$ is a probability density function, symmetric around zero, and uniformly continuous on \mathbb{R} . Furthermore, defining $K_{jk} = \int_{\mathbb{R}} K(u)^j u^k du$ for $j, k \in \mathbb{N}$, $|K_{14}|$ and $|K_{26}|$ are both finite. The derivative K' exists and is bounded on the support of K , i.e., $\sup_{K(x)>0} |K'(x)| < \infty$; additionally, $\int_{\mathbb{R}} x^2 |K'(x)| (|x \log |x||)^{1/2} dx < \infty$.

(A4) $f_Z(\cdot)$ and $f_{Z|\nu}(\cdot, \mu)$ both exist and are continuous on \mathcal{T} and twice continuously differentiable on \mathcal{T}° , the latter for all $\mu \in \mathcal{W}$. The marginal density $f_Z(\cdot)$ is bounded away from zero on \mathcal{T} , $\inf_{z \in \mathcal{T}} f_Z(z) > 0$. The second-order derivative f_Z'' is bounded, $\sup_{z \in \mathcal{T}^\circ} |f_Z''(z)| < \infty$. The second-order partial derivatives $(\partial^2 f_{Z|\nu} / \partial z^2)(\cdot, \mu)$ are uniformly bounded, $\sup_{z \in \mathcal{T}^\circ, \mu \in \mathcal{W}} |(\partial^2 f_{Z|\nu} / \partial z^2)(z, \mu)| < \infty$. Additionally, for any open set $U \subset \mathcal{W}$, $\int_U dF_{\nu|Z}(z, \mu)$ is continuous as a function of z ; for any $z \in \mathcal{T}$, $M(\mu, z) = E\{d_{\mathcal{W}}^2(\nu, \mu) | Z = z\}$ is equicontinuous, i.e.,

$$\limsup_{x \rightarrow z} \sup_{\mu \in \mathcal{W}} |M(\mu, x) - M(\mu, z)| = 0.$$

References

- Anderson, S. E. and Whitaker, R. C. (2009) Prevalence of obesity among US preschool children in different racial and ethnic groups. *Archives of Pediatrics & Adolescent Medicine*, **163**, 344–348.
- Bigot, J., Gouet, R., Klein, T. and López, A. (2017) Geodesic PCA in the Wasserstein space by convex PCA. *Annales de l'Institut Henri Poincaré B: Probability and Statistics*, **53**, 1–26.
- Bigot, J., Gouet, R., Klein, T. and Lopez, A. (2018) Upper and lower risk bounds for estimating the Wasserstein barycenter of random measures on the real line. *Electronic Journal of Statistics*, **12**, 2253–2289.
- Bonevski, B., Randell, M., Paul, C., Chapman, K., Twyman, L., Bryant, J., Brozek, I. and Hughes, C. (2014) Reaching the hard-to-reach: a systematic review of strategies for improving health and medical research with socially disadvantaged groups. *BMC Medical Research Methodology*, **14**, 1–29.
- Chen, Y., Gajardo, A., Fan, J., Zhong, Q., Dubey, P., Bhattacharjee, S., Han, K. and Müller, H. (2020) *frechet: statistical analysis for random objects and non-Euclidean data*. R package version 0.2. 0.

- Chen, Y., Lin, Z. and Müller, H.-G. (2023) Wasserstein regression. *Journal of the American Statistical Association*, **118**, 869–882.
- Chen, Y. and Müller, H.-G. (2022) Uniform convergence of local Fréchet regression, with applications to locating extrema and time warping for metric-space valued trajectories. *Annals of Statistics*, **50**, 1573–1592.
- Danielzik, S., Czerwinski-Mast, M., Langnäse, K., Dilba, B. and Müller, M. (2004) Parental overweight, socioeconomic status and high birth weight are the major determinants of overweight and obesity in 5–7 y-old children: baseline data of the Kiel Obesity Prevention Study (KOPS). *International Journal of Obesity*, **28**, 1494–1502.
- Fletcher, P. T. (2013) Geodesic regression and the theory of least squares on Riemannian manifolds. *International Journal of Computer Vision*, **105**, 171–185.
- Fréchet, M. (1948) Les éléments aléatoires de nature quelconque dans un espace distancié. *Annales de l'Institut Henri Poincaré*, **10**, 215–310.
- Gajardo, Á. and Müller, H.-G. (2021) Cox point process regression. *IEEE Transactions on Information Theory*, **68**, 1133–1156.
- Ghodrati, L. and Panaretos, V. M. (2022) Distribution-on-distribution regression via optimal transport maps. *Biometrika*, **109**, 957–974.
- Gillman, M. (2022) Environmental Influences on Child Health Outcomes (ECHO)-wide Cohort. NICHD Data and Specimen Hub. <https://dash.nichd.nih.gov/study/417122>. URL: <https://dash.nichd.nih.gov/study/417122>.
- Gillman, M. W. and Blaisdell, C. J. (2018) Environmental influences on Child Health Outcomes, a research program of the NIH. *Current Opinion in Pediatrics*, **30**, 260.
- Hron, K., Menafoglio, A., Templ, M., Hruzova, K. and Filzmoser, P. (2016) Simplicial principal component analysis for density functions in Bayes spaces. *Computational Statistics and Data Analysis*, **94**, 330–350.
- Jank, W. and Shmueli, G. (2010) *Modeling Online Auctions*. John Wiley & Sons.
- Kantorovich, L. V. (1942) On the translocation of masses. *Dokl. Akad. Nauk SSSR* (translated version in *Journal of Mathematical Sciences*, 133, 1381–1382, 2006), **37**, 227–229.

- Kloeckner, B. (2010) A geometric study of Wasserstein spaces: Euclidean spaces. *Annali della Scuola Normale Superiore di Pisa-Classe di Scienze*, **9**, 297–323.
- Knapp, E. A., Kress, A. M., Parker, C. B., Page, G. P., McArthur, K., Gachigi, K. K., Alshawabkeh, A. N., Aschner, J. L., Bastain, T. M., Breton, C. V. et al. (2023) The Environmental influences on Child Health Outcomes (ECHO)-wide Cohort. *American Journal of Epidemiology*, in press.
- Liu, B. and Müller, H.-G. (2009) Estimating derivatives for samples of sparsely observed functions, with application to on-line auction dynamics. *Journal of the American Statistical Association*, **104**, 704–714.
- Liu, W. W., Liu, Y. and Chan, N. H. (2019) Modeling eBay price using stochastic differential equations. *Journal of Forecasting*, **38**, 63–72.
- Niles-Weed, J. and Berthet, Q. (2022) Minimax estimation of smooth densities in Wasserstein distance. *Annals of Applied Statistics*, **50**, 1519–1540.
- O’Connor, M., Spry, E., Patton, G., Moreno-Betancur, M., Arnup, S., Downes, M., Goldfeld, S., Burgner, D. and Olsson, C. A. (2022) Better together: Advancing life course research through multi-cohort analytic approaches. *Advances in Life Course Research*, 100499.
- Panaretos, V. M. and Zemel, Y. (2016) Amplitude and phase variation of point processes. *Annals of Statistics*, **44**, 771–812.
- (2020) *An Invitation to Statistics in Wasserstein Space*. Springer New York.
- Pegoraro, M. and Beraha, M. (2022) Projected statistical methods for distributional data on the real line with the Wasserstein metric. *Journal of Machine Learning Research*, **23**, 37–1.
- Petersen, A., Liu, X. and Divani, A. A. (2021) Wasserstein F -tests and confidence bands for the Fréchet regression of density response curves. *Annals of Statistics*, **49**, 590–611.
- Petersen, A. and Müller, H.-G. (2016) Functional data analysis for density functions by transformation to a Hilbert space. *Annals of Statistics*, **44**, 183–218.
- (2019) Fréchet regression for random objects with Euclidean predictors. *Annals of Statistics*, **47**, 691–719.

- Petersen, A., Zhang, C. and Kokoszka, P. (2022) Modeling probability density functions as data objects. *Econometrics and Statistics*, **21**, 159–178.
- Qiu, J., Dai, X. and Zhu, Z. (2022) Nonparametric estimation of repeated densities with heterogeneous sample sizes. *Journal of the American Statistical Association*, 1–13.
- Stellato, B., Banjac, G., Goulart, P., Bemporad, A. and Boyd, S. (2020) OSQP: An operator splitting solver for quadratic programs. *Mathematical Programming Computation*, **12**, 637–672.
- Talská, R., Menafoglio, A., Machalová, J., Hron, K. and Fišerová, E. (2018) Compositional regression with functional response. *Computational Statistics & Data Analysis*, **123**, 66–85.
- Vazquez, C. E. and Cubbin, C. (2020) Socioeconomic status and childhood obesity: a review of literature from the past decade to inform intervention research. *Current Obesity Reports*, **9**, 562–570.
- Villani, C. (2003) *Topics in Optimal Transportation*. American Mathematical Society.
- Wang, S., Jank, W., Shmueli, G. and Smith, P. (2008) Modeling price dynamics in eBay auctions using principal differential analysis. *Journal of the American Statistical Association*, **103**, 1100–1118.
- Zhang, C., Kokoszka, P. and Petersen, A. (2022) Wasserstein autoregressive models for density time series. *Journal of Time Series Analysis*, **43**, 30–52.
- Zhu, C. and Müller, H.-G. (2023) Autoregressive optimal transport models. *Journal of the Royal Statistical Society Series B: Statistical Methodology*, **85**, 1012–1033.